Synthesis of PANI@ZnO Hybrid Material and Evaluations in Adsorption of Congo Red and Methylene Blue Dyes: Structural Characterization and Adsorption Performance

Imane Toumi
Abdelhamid Ibn Badis University of Mostaganem
Halima Djelad
Abdelhamid Ibn Badis University of Mostaganem
Faiza Chouli
Abdelhamid Ibn Badis University of Mostaganem
Benyoucef Abdelghani (abdelghani@ua.es)
Faculté des Sciences et Thechnologie https://orcid.org/0000-0002-0247-2808

Research Article

Keywords: PANI, ZnO, Nanocomposite, Congo Red, Methylene Blue, Removal

Posted Date: June 30th, 2021

DOI: https://doi.org/10.21203/rs.3.rs-661310/v1

Version of Record: A version of this preprint was published at Journal of Inorganic and Organometallic Polymers and Materials on August 7th, 2021. See the published version at https://doi.org/10.1007/s10904-021-02084-0.

Synthesis of PANI@ZnO hybrid material and evaluations in adsorption of Congo red and Methylene blue dyes: Structural characterization and adsorption performance

I. Toumi [1], H. Djelad [2,3], F. Chouli [1], A. Benyoucef [2 *]

[1]*Faculty of Science and Technology; Abdelhamid Ibn Badis University of Mostaganem. Algeria*

[2] *LMAE Laboratory; University of Mustapha Stambouli Mascara, Algeria*

[3]*University Materials Institute of Alicante (IUMA); University of Alicante, Spain*

[*]Corresponding author : abdelghani@ua.es or a.benyoucel@univ-mascara.dz

Abstract

In this research, a simple oxidation chemical process was applied for the synthesis of novel PANI@ZnO nanocomposite. The prepared nanocomposites were characterized by XPS, XRD, FTIR, SEM, TGA and N_2 adsorption-desorption isotherms. Thereby, PANI@ZnO highest S_{BET} values (about 40.84 $m^2.g^{-1}$), total mesoporous volume (about 3.214 $cm^3.g^{-1}$) and average pore size (about 46.12 nm). Afterwards, the prepared nanomaterial was applied as novel nanoadsorbent for the adsorption of Congo Red (CR) and Methylene Blue (MB) dyes from aqueous solutions at 298 K and pH 5.0. Besides, the pseudo-second-order model was obtained the best for the adsorption of both dyes. In the case of isotherm models, the Freundlich model showed the best fit. After removal, the spent adsorbent was regenerated. With the regeneration repeated five cycles, the PANI@ZnO regeneration efficiency remained at a very adequate level.

Keywords: PANI; ZnO; Nanocomposite; Congo Red; Methylene Blue; Removal.

1. Introduction

Dye effluents are one of the most dangerous chemical product classes found in industrial textile waste to the environment. These dyes can cause dermatitis, allergy and too provoke cancer [1-3]. Therefore, its elimination from different aqueous wastes is required and necessary to protect environment and human health. Generally, membrane filtration process, precipitation, coagulation, biological treatment, precipitation, adsorption, ion exchange, electrochemical process, photocatalytic degradation and ozonation are adequate candidates for such purpose [4-11]. In addition, adsorption treatment is the most effective method because providing the simplicity in employment, flexibility and low cost [12].

Similarly to conducting polymer, polyaniline (PANI) is a popular. This conductive product also has other appealing features such as good environmental stability, simple synthesis, ability to dope with protonic acids, and the being of amine groups in its structure and higher electrical conductivity [13-15]. The polyaniline has been prepared via chemical oxidative polymerization and electropolymerization process [16-19]. Generally, the usage of PANI is presently limited, due to its poor mechanical property. The PANI nanocomposites with different inorganic materials greatly ameliorate their physical and structural properties for pertinent applications [20-22]. Among the inorganic nanomaterials, ZnO nanoparticles have received vast interest in exclusive electrical, photocatalytic, adsorption, electronic and optical properties due to their wide bandgap (3.31 eV) as well as their low cost [23, 24]. Several synthesis methods have been widely used for the synthesis of the hybrid materials of PANI with ZnO [17]. Additionally, PANI@inorganic hybrid is already an established adsorbent of organic pollutants in aqueous solution, such as Orange G, Methyl orange, Methylene blue, Malachite green, Congo red, Amido black 10B [25-29], etc.

This investigation aims to demonstrate the synthesis and application of PANI@ZnO by in-situ chemical oxidative process. The adsorbent product was characterized by different techniques XPS, XRD, FT-IR, SEM, TGA and BET. The removal of Congo red (CR) and Methylene blue (MB) using PANI@ZnO adsorbent was studied. The process of adsorption was established through the kinetics, isotherm and regeneration results.

2. Experimental

2.1. Materials

Congo red (CR) and Methylene blue (MB), Aniline (ANI), Ammonium persulfate (APS), Zinc oxide ZnO (> 99%), Hydrochloric acid 37% and Ethanol 96% made by Merck Company. Deionized H_2O was used for all experiments.

2.2. Measurements

FTIR Spectrometer (Bruker-Inc., Model-Alpha spectrophotometer) was applied to determine the functional groups. XRD (Bruker-CCD Apex instrument) was applied to determine the structural properties of samples. Calculation of the specific surface area was performed by N_2 adsorption & desorption analysis (Autosorb-6-Quantachrome equipment). UV-Spectrophotometer (Hitachi U-3000 Spectrophotometer) was applied to measure the MO concentration. (SEM) images of the products were taken using (FEI Quanta 400 FEG). Thermogravimetry Analyze (TGA) (Hitachi STA7200 Instrument) was used to determine the thermal and/or oxidative stabilities of materials as well as their. X-ray photoelectron spectroscopy analysis (XPS) was controlled by (VG Microtech Multilab 3000-electron) spectrometer. [20, 30].

2.2.1. Porous texture characterization

The microscopic pore structure property of adsorbent was characterized by physical adsorption of gases (nitrogen at 77K & Carbon dioxide at 273K) using Micromeritics ASAP-2020M system. Correspondingly, N_2 adsorption is mainly to gain the information on total micropores volume (V_{DR}) applying the Dubinin–Radushkevich (DR) formula and to determine the specific surface area according to the BET law (S_{BET}) [25, 31].

2.3. Synthesis of adsorbent material

Adsorbent material was synthetized by insitu polymerization of ANI 220 mol in HCl dispersions of ZnO nanoparticles. 1.0 g of ZnO was added to a 0.5M HCl and sonicated using probe ultrasound for 30 min. Thereafter, the ANI was added, and the solution was sonicated also 30 min to prepare stable suspension. Finally, APS dissolved in 0.5M of HCl was added dropwise to solution of ANI with ZnO under constant stirring (the molar ratio of ANI to APS was 1:1). The preparation was carried out at 298 K for 24h. The final produced were filtered, washed with deionized H_2O and then dried in oven at 333 K for 24h [20, 30-32]. The PANI was synthetized in similar way mentioned above but in absence of ZnO.

2.4. Adsorption tests

The 1000ppm stock dyes (CR or MB) solution was synthesized through dissolving 1.0 g of CR powder in 1 L of deionized H_2O. Then, through dilution, the solution was synthesized with the required initial concentrations of dyes from 5 to 200 ppm.

2.4.1. Batch adsorption experiments

Kinetics of batch adsorption experiments were considered to investigate the time to reach equilibrium and carried out at dyes (CR or MB) solution concentrations of 5ppm, 10ppm, 50ppm, 100ppm, 150ppm and 200ppm with 10 mg of the PANI@ZnO adsorbent in the ambient temperature. The CR and MB solution concentration was identifying by UV–Vis

spectrophotometer in wavelength of maximum absorbance of 497 nm and 664 nm, respectively. A calibration curve of concentration-vs-absorbance was determined by Beer–Lambert's equation. The quantity of dyes adsorbed at equilibrium, Q_{eq} (mg.g^{-1}), was established applied formula below:

$$Q_{eq} = \frac{(C_0 - C_{eq})V}{m}$$

Here, m (g) is the amount of adsorbent; C_0 and C_{eq} (mg.L^{-1}) are the initial and equilibrium concentrations of dye, respectively; V (mL) is dye volume; Q_{eq} (mg.g^{-1}) is the quantity of dye adsorbed by adsorbent at time t.

The needful properties of the Langmuir model can be proved in terms of a dimensionless separation factor (R_L) are obtained by the following:

$$R_L = \frac{1}{1 + K_L C_0}$$

Here, C_0: the dye concentration at equilibrium (mg.L^{-1}) and K_L: the Langmuir constant (L.mg^{-1}). R_L shows the state of isotherm to be either unfavorable for $R_L > 1$, favorable ($0 < R_L < 1$), linear for $R_L = 1$ or irreversible for $R_L = 0$ [33].

In conformity with the Freundlich isotherm, the adsorbed molecules cannot be greater than of active sites number, and the layer formed on nanoadsorbent surface authorized development of following layers [34]. The isotherm is determined by the next law:

$$logQ_{eq} = logK_F + \frac{1}{n} logC_{eq}$$

Here, K_F : Freundlich-constant (L.mg^{-1}) ; $^1/_n$: intensity of adsorption constant ; Q_{eq} : adsorption capacity of dye adsorbed at equilibrium (mg.g^{-1}) and C_{eq} : equilibrium concentration of dye (mg.L^{-1}).

Adsorption kinetic isotherms were used to describe adsorptive molecules transfer behavior and investigate factors affecting reaction rate. In the current work, pseudo first order (PFO) and pseudo second order (PSO) kinetics models were applied to research the batch adsorption performance.

PFO:

$$\log(Q_{eq} - Q_t = logQ_{eq} - \frac{k_l}{2.303}$$

PSO:

$$\frac{1}{Q_t} = \frac{1}{k_2 Q_{eq}^2} + \frac{1}{Q_{eq}} t$$

Here, Q_{eq} is quantity of dye adsorbed (mg.g^{-1}) ; Q_t is dye quantity on adsorbent surface at every time t (mg.g^{-1}) and k is equilibrium speed-constant of the PFO.

2.4.2. Adsorbent regeneration test

From the operational perspective and environmental goals, adsorbent regeneration and reuse constitute one of the important and innovative aspects of economic feasibility. To investigate PANI@ZnO adsorbent regeneration performance, 0.1 g of the prepared adsorbent was poured in 25 ml of dye (CR or MB) solution with a concentration of 150ppm at 298 K under stirring for 2 h. The residue dye solution concentration was determined by UV-Vis spectrophotometer and dye adsorption capacity by PANI@ZnO was investigated.

147 After that, the adsorbent was removed from the solution and placed in 40 ml of nitric
148 acid 0.05 molar as elution solvent on a stirrer for 10 minutes. Afterwards, the PANI@ZnO
149 adsorbent was washed with deionization H_2O and placed in dye solution with the same
150 condition and these stages were repeated for 5 cycles.

151 **3. Results and Discussion**

152 ***3.1. Adsorbent characterization***

153 To further characterize micromorphology and molecular structure of the products, XPS,
154 XRD, FITR, TGA, SEM and BET measurements were carried out. Fig. 1-a show the XPS
155 wide survey-spectra of the ZnO sample give the characteristic peaks of Zn3d, Zn3p, Zn3s, C1s,
156 O1s, Zn2p3 and Zn2p1 with the corresponding binding energies of 21.41 eV, 72.94 eV, 141.57
157 eV, 285.57 eV, 532.22 eV, 1021.35 eV and 1044.83 eV, respectively [35]. As demonstrated in
158 Table 1, the high resolution XPS spectrum of Zn2p3 presented shows three evident signals
159 located at 1021.69 eV, 1022.45 eV and 1023.62 eV are arising from the Zn metal, Zn–O and
160 $Zn(OH)_2$, respectively. Moreover, the XPS spectrum of PANI shows the C1s, N1s and O1s. On
161 the one hand, analysis of the high-resolution N1s spectra using a peak of deconvolution (Table
162 1), revealed two functional groups around 399.70 eV (=N–) and 400.74 eV (–NH–).
163 Furthermore, the C1s spectrum contained three contributions at 284.60 eV (C–H, C–C or C=C),
164 285.92 eV (C–O/C–N) and 287.22 eV (N–C=N). These assignments of the mentioned
165 functional groups are in agreement with the literature [21]. Likewise, the XPS spectra confirm
166 that Zn and N elements exists mainly in the form PANI@ZnO surfaces, this indicating to
167 successful formation of hybrid materials

Fig. 1-b. display the FT-IR spectrum of synthesized PANI, it can be seen a series of characteristic peaks including C=C stretching vibration of benzenoid units at 1500 cm^{-1} and 1589 cm^{-1} of PANI are presented [20, 21], which makes clear that the PANI is in semi-oxidation state. The band at 1239 cm^{-1} is attributed to C–N stretching vibration of secondary aromatic amino structures [36]. The main characteristic band at 750 cm^{-1} is belonging to the aromatic N–H stretching vibration of secondary aromatic amine bending vibration. Moreover, the main band at 1111 cm^{-1} is attributed to the out-of-plane bending vibration of C–H within the stretching vibration of C–N of the secondary aromatic amine structures bending vibration. Besides, the ZnO nanoparticles display one maximum at 537 cm^{-1} [37, 38]. Additional absorption bands were attributed to organic impurities originating from reaction intermediates, whilst one at 3438 cm^{-1} was ascribed to the OH-group on ZnO surface. Moreover, the FTIR spectra of PANI@ZnO are which fully match PANI spectra. Therefore, the bands at 1602 and 1500 cm^{-1} are ascribed to vibrations of quinoid & benzene rings, respectively. The other characteristic bands at 1302, 1104, 792 and 697 cm^{-1} can be attributed with the C–N stretching of the secondary aromatic amine, aromatic C–H in-plane and out-of-plane bending, respectively. Furthermore, the band of ZnO at 537 cm^{-1} are shifted to 569 cm^{-1}, indicating the formation of PANI@ZnO hybrid. Generally, this results show a clear shifting of wavenumbers indicating the interaction between PANI and the surface of the ZnO

The XRD patterns of the PANI, ZnO and PANI@ZnO samples, respectively (Fig. 1-c). The ZnO shows peaks at 2θ = 31.78º, 34.38º, 36.24º, 47.53º, 56.63º, 62.87º and 67.91º belong to (100), (002), (101), (102), (110), (103) and (112) crystal planes according to JCPSD card no. 01-007-2551. Moreover, the PANI, being semi crystalline in nature, showed two sharp bands centered at 2θ = 7.43º and 24.17º corresponding to (002) and (200) crystal planes, with and a

broad band indicating that the majority of PANI chains were oriented in these crystal planes. Also, broad a peak are observed between 2θ = 13.18º to 18.28º indexed to (011) and (020). On the other hand, PANI@ZnO shows two peaks at 2θ = 31.81º and 36.24º corresponding to the reflections due to the ZnO (100) and (101) planes. The peak at 2θ = 7.78º of hybrid material also coincided with the (002) peak of pure PANI, but in contrast to PANI, the XRD peak of PANI@ZnO converted to a broad amorphous peak that is observed between 2θ = 15.54º to 30.53º. By comparing the XRD patterns of the hybrid adsorbent and ZnO, it is assured that ZnO nanoparticles has retained its structure even though it is dispersed in polymer matrix during synthesis reaction.

The TGA curve of PANI, ZnO and PANI@ZnO were showed in Fig. 1-d. PANI displayed the initial weight loss (10.21%) below 266 ºC, which was attributed to the loss of H_2O and solvents molecules. The second weight loss (42.51%) in the range from 266 ºC to 447 ºC was due to the removal of structural organic ligands from their frameworks. At 900 ºC, the total weight loss of PANI was 66.21%, while PANI@ZnO was 50.51%. The reason is that the presence of PANI on the surface of ZnO promoted the growth of the crystal. It was concluded that PANI@ZnO had better thermal stability than polymer, mainly due to the introduction of ZnO in PANI matrix.

The SEM images of samples are shown in Fig. 2. The ZnO nanoparticles were grain and it has the shape of faceted crystals [39]. This material is characterized by adequate porosity. While, PANI shows a classically cauliflower-like morphology [40]. Whereas that, the SEM images clearly exhibit the dual structure of PANI@ZnO hybrid that is comprised of spherical particles are surrounded by polymer matrix and hence it appears as agglomerated macromolecules [41].

The textural properties of PANI and PANI@ZnO were calculated by BET Nitrogen adsorption-desorption isotherms determined and the obtained values is described in Table 2 and Fig. 3-a. It is found that the measurement S_{BET} of PANI@ZnO was increased in some extent due to existence of ZnO nanoparticles, indicating large ratio of macropores in hybrid adsorbent. The textural characteristic of PANI@ZnO is more favorable to the adsorption of dyes [42].

3.2. Adsorption of MO

3.2.1. Influence of pH

The effect the pH solution has on the dyes (CR or MB) removal was investigated by modifying the reaction solution pH from 4 to 11 and conserving all other parameters constant by PANI@ZnO adsorbent. Herein, lower pHs were not tested due to the instability of CR below pH 5 [43]. Fig. 3-b shows the effect pH has on removal efficiency. It is clear that PANI@ZnO performed better in the adsorption of CR from aqueous solution at various values of pH compared with MB dye. As observed, the adsorbent hybrid has a high potential for both dyes removal on the pH between 5 and 6. Furthermore, as Emeraldine-Salt (ES) and Emeraldine-Base (EB) formulas of the PANI in adsorbent hybrid occur at lower acidic and higher basic pH values respectively, the ES form get passed to EB about pH 7 [44]. Accordingly, the decrease in the dyes removal efficiency is may be related to this phenomenon that the surface of the PANI@ZnO adsorbent becomes less positive when pH increased from 5 to 11. The negative charge on the surface of adsorbents promotes repelling of negatively charged dyes. Therefore, pH 5 was selected for further experiments.

3.2.2. Effect of adsorption time on adsorption efficiency

Fig. 3-c. exhibits a comparison of the CR and MB dyes adsorption capacity by PANI@ZnO adsorbent and removal efficiency with time. The results displayed that the %removal of CR increased with increasing time from 10 to 40 min where reached 19.23 % at 40 min. Thereafter, the %removal of CR increased to 81.37 % when the time changed from 40 to 60 min. Also, the influence of time on the adsorption capacity of PANI@ZnO adsorbent toward MB was performed in the time range of 10-120 min. The results also showed that the adsorption capacity toward MB increased with increasing time from 10 to 60 min where reached 59.23 $mg.g^{-1}$ (76.48 %) at 60 min. Hence, longer times had no significant effect on the results which revealed a relatively fast adsorption process. Based on the obtained results, a time of 60 min was selected as the equilibrium time for further experiments.

To prepare information about factors affecting reaction rate, it is necessary to determine mechanisms that control the adsorption process such as surface adsorption, chemical reaction, and kinetics assessment infiltration mechanisms. PFO and PSO models have widely used for investigation of the adsorption process. In Table 3, the parameters related to studied kinetic models are presented. Accordingly, the PSO kinetic model provided the best results regarding R^2 value which proposes a physiochemical adsorption process and an intraparticle diffusion mechanism for both dyes. The obtained R^2 values for PSO model were 0.977 and 0.991 for CR and MB dyes, respectively. Also, the calculated value of $Q_{eq.Cal}$ obtained from the PSO model is close to the experimental value of $Q_{eq.Exp}$. Hence, the kinetics of adsorption is best defined by the PSO kinetic model for both dyes used in this study.

3.3. Adsorption isotherms of dyes

Fig. 3-d. displays the adsorption isotherms of both dyes (CR or MB) by PANI@ZnO nanoadsorbent calculated at 298 K. The matching result of sorption isotherms using Langmuir and Freundlich models are summarized in Table 4. The data show that the removal process of dyes was fitted well with the Langmuir isotherm. Likewise, this isotherm model indicates heterogeneous and multilayer adsorption sites. Further, the removal capacity toward CR and MB by PANI@ZnO are 69.82 $mg.g^{-1}$ and 56.23 $mg.g^{-1}$, respectively. To compare the present method with other reported studies for the adsorption of CR or MB, adsorption capacity of the methods is summarized in Table 5. Thus, the present study provided better adsorption capacity in comparison with other reported methods using adsorbent. One possible reason for the better performance of the prepared adsorbents is the adsorption mechanism, which occurs in both anion exchange and surface adsorption by H-bonding with π-π liaison.

3.4. Reuse of adsorbent

Regeneration and reusability of an adsorbent material is an important factor to assess the feasibility for workable applications. Therefore, this adsorbent product was used for several adsorption-regeneration cycles with removal over 60 min. In this study, washing of employed adsorbent with C_2H_5OH and distilled H_2O was used to regenerate the adsorbent PANI@ZnO. As shown in Fig. 4. the adsorbent present suitable capabilities for recovery and reuse. Besides, the adsorbent recovery at some steps showed a stable adsorbent capacity in dye removal which this result can illustrate that C_2H_5OH is an exceptional detergent for adsorbent recovery. On the other hand, the continuous decrease in quantity adsorbed and reusability efficiency could suggest that some dyes remained on adsorbent material next each reusability or that the adsorbent structure was changing.

4. Conclusions

In this research, PANI@ZnO nanocomposite was facilely prepared by in-situ oxidative polymerization. After the characterization of the synthesized nanocomposite by XPS, XRD, FTIR, TGA, SEM and BET analyses, this hybrid material were applied as novel adsorbent for removal of CR and MB dyes from aqueous solution. The effect of important experimental parameters including solution pH, contact time, dyes concentration, kinetics, and isothermal analysis was investigated. The novel prepared nanoadsorbent showed significant adsorption performance toward both dyes. Moreover, the kinetic analysis detected that PSO rate formula executed better than PFO rate law, this promoting the formation of physiochemical adsorption process and an intraparticle diffusion mechanism. For isothermal studies, the Freundlich model showed the best fit based on R^2 values. Finally, maximum adsorption capacities of 69.82 $mg.g^{-1}$ and 59.23 $mg.g^{-1}$ were obtained for CR and MB dyes, respectively, by PANI@ZnO adsorption. Additionally, the obtained nanoadsorbent exhibited an adequate cyclability to a range between 77.14% and 40.34% after 5 cycles.

Acknowledgements

Authors gratefully acknowledge the Algerian Ministry of Higher Education and Scientific Research, and also University Materials Science Institute of Alicante Spain for the co-operation availing.

Funding information: There is no financial sources funding regarding of this study.

Conflict of Interest: The authors declare that they have no competing interests.

299 **References**

300 [1] R. Pandimurugan, S. Thambidurai. Synthesis of seaweed-ZnO-PANI hybrid composite for
301 adsorption of methylene blue dye. Journal of Environmental Chemical Engineering. 4
302 (2016) 1332-1347.

303 [2] D.S. Brookstein. Factors Associated with textile pattern dermatitis caused by contact allergy
304 to dyes finishes, foam and preservatives. Dermatologic Clinics. 27 (2009) 309-322

305 [3] P.A. Carneiro, G.A. Umbuzeiro, D.P. Oliveira, M.V.B. Zanoni. Assessment of water
306 contamination caused by a mutagenic textile effluent/dye house effluent bearing disperse
307 dyes. Journal of Hazardous Materials. 174 (2010) 694-699.

308 [4] P. Mokhtari, M. Ghaedi, K. Dashtian, M.R. Rahimi, M.K. Purkait. Removal of methyl
309 orange by copper sulfide nanoparticles loaded activated carbon: Kinetic and isotherm
310 investigation. Journal of Molecular Liquids. 219 (2016) 299-305.

311 [5] B.A.M. Al-Rashdi, D.J. Johnson, N. Hilal. Removal of heavy metal ions by nanofiltration.
312 Desalination, 315 (2013) 2-17.

313 [6] S. Dashamiri, M. Ghaedi, K. Dashtian, M.R. Rahimi, A. Goudarzi, R. Jannesar. Ultrasonic
314 enhancement of the simultaneous removal of quaternary toxic organic dyes by CuO
315 nanoparticles loaded on activated carbon: Central composite design, kinetic and isotherm
316 study. Ultrasonics Sonochemistry. 31 (2016) 546-557.

317 [7] A. Paz, J. Carballo, M.J. Perez, J.M. Dominguez. Biological treatment of model dyes and
318 textile wastewater. Chemosphere. 181 (2017) 168-177

[8] S. Sachdeva, A. Kumar. Preparation of nanoporous composite carbon membrane for separation of rhodamine B dye. Journal of Membrane Science. 329 (2009) 2-10.

[9] A. Asfaram, M. Ghaedi, S Hajati, A. Goudarzi, A.A. Bazrafshan. Simultaneous ultrasound-assisted ternary adsorption of dyes onto copper-doped zinc sulfide nanoparticles loaded on activated carbon: Optimization by response surface methodology. Spectrochimica Acta Part A: Molecular and Biomolecular Spectroscopy. 145 (2015) 203-212.

[10] K. Dai, H. Chen, T. Peng, D. Ke, H. Yi. Photocatalytic degradation of methyl orange in aqueous suspension of mesoporous titania nanoparticles. Chemosphere. 69 (2007) 1361-1367.

[11] A. Asfaram, M. Ghaedi, S. Hajati, M. Rezaeinejad, A. Goudarzi, M.K. Purkait. Rapid removal of Auramine-O and Methylene blue by ZnS:Cu nanoparticles loaded on activated carbon: A response surface methodology approach. Journal of the Taiwan Institute of Chemical Engineers. 53 (2015) 80-91.

[12] G. Crini. Non-conventional low-cost adsorbents for dye removal: a review. Bioresour. Technol., 97 (2006) 1061-1085.

[13] H. Wu, S. Lin, C. Chen, W. Liang, X. Liu, H. Yang.A new ZnO/rGO/polyaniline ternary nanocomposite as photocatalyst with improved photocatalytic activity.Materials Research Bulletin. 83 (2016) 434-441.

[14] C. Chen, T. Xu, A. Chen, L. Lu, Y. Gao. Electrosynthesis of poly(N-methylthionine)/polyaniline nanocomposites with enhanced electrochemical and electrocatalytic activities. Journal of the Electrochemical Society. 163 (2016) G159-G165

340 [15] A. Eftekhari. Nanostructured Conductive Polymers. John Wiley & Sons (2011).

341 [16] X. Zheng, M.E.A. Mohsin, A. Arsad, A. Hassan. Polymerization of polyaniline under
342 various concentrations of ammonium peroxydisulfate and hydrochloric acid by ultrasonic
343 irradiation. Journal of Applied Polymer Science. 138 (2021) 50637.

344 [17] S. Daikh, F. Z. Zeggai, A. Bellil, A. Benyoucef. Chemical polymerization, characterization
345 and electrochemical studies of PANI/ZnO doped with hydrochloric acid and/or zinc
346 chloride: Differences between the synthesized nanocomposites. Journal of Physics and
347 Chemistry of Solids. 121 (2018) 78-84.

348 [18] M. Zhang, A. Nautiyal, H. Du, Z. Wei, X. Zhang, R. Wang. Electropolymerization of
349 polyaniline as high-performance binder free electrodes for flexible supercapacitor.
350 Electrochimica Acta. 376 (2021) 138037.

351 [19] D.S. Torres, F. Montilla, F. Huerta, E. Morallón. All electrochemical synthesis of
352 polyaniline/silica sol–gel materials. Electrochimica Acta. 56 (2011) 3620-3625.

353 [20] L. Maaza, F. Djafri, A. Belmokhtar, A. Benyoucef. Evaluation of the influence of Al2O3
354 nanoparticles on the thermal stability and optical and electrochemical properties of PANI-
355 derived matrix reinforced conducting polymer composites. Journal of Physics and
356 Chemistry of Solids. 152 (2021) 109970.

357 [21] M.A. Bekhti, M.S. Belardja, M. Lafjah, F. Chouli, A. Benyoucef. Enhanced tailored of
358 thermal stability, optical and electrochemical properties of PANI matrix containing Al_2O_3
359 hybrid materials synthesized through in situ polymerization. Polymer Composites. 42
360 (2021) 6-14.

[22] M.S. Belardja, H. Djelad, M. Lafjah, F. Chouli, A. Benyoucef. “The influence of the addition of tungsten trioxide nanoparticle size on structure, thermal, and electroactivity properties of hybrid material-reinforced PANI”. Colloid and Polymer Science. 298 (2020) 1455-1463.

[23] I. Litty, V.P.N. Nampoori, P. Radhakrishnan. Optical Limiting in ZnO Nanocomposites. Science of Advanced Materials. 2 (2010) 578-582.

[24] L. Hongjun, Z. Zang, X. Tang. Synthesis mechanism and optical properties of well nanoflower-shaped ZnO fabricated by a facile method. Optical Materials Express. 4 (2014) 1762-1769.

[25] O. Mahi, K. Khaldi, M. S. Belardja, A. Belmokhtar, A. Benyoucef. Development of a New Hybrid Adsorbent from Opuntia Ficus Indica NaOH Activated with PANI Reinforced and Its Potential Use in Orange G Dye Removal. Journal of Inorganic and Organometallic Polymers and Materials. 31 (2021) 2095-2104.

[26] R. Saravanan, E. Sacari, F. Gracia, M.M. Khan, E. Mosquera, V.K. Gupta. Conducting PANI stimulated ZnO system for visible light photocatalytic degradation of coloured dyes. Journal of Molecular Liquids. 221 (2016) 1029-1033.

[27] V. Eskizeybek, F. Sarı, H. Gülce, A. Gülce, A. Avcı. Preparation of the new polyaniline/ZnO nanocomposite and its photocatalytic activity for degradation of methylene blue and malachite green dyes under UV and natural sun light irradiations. Applied Catalysis B: Environmental. 119-120 (2012) 197-206

[28] R. Kumar, S.A. Ansari, M.A. Barakat, A. Aljaafari, M.H. Cho. A polyaniline@MoS2-based organic–inorganic nanohybrid for the removal of Congo red: adsorption kinetic, thermodynamic and isotherm studies. New Journal of Chemistry. 40 (2018) 18802-18809

[29] R. Ahmad, R. Kumar. Conducting Polyaniline/Iron Oxide Composite: A Novel Adsorbent for the Removal of Amido Black 10B. Journal of Chemical & Engineering Data. 55 (2010) 3489-3493.

[30] F. Z. Kouidri, I. Moulefera, S. Bahoussi, A. Belmokhtar, A. Benyoucef. Development of hybrid materials based on carbon black reinforced poly(2-methoxyaniline): preparation, characterization and tailoring optical, thermal and electrochemical properties. Colloid and Polymer Science (2021). doi.org/10.1007/s00396-021-04837-2.

[31] A. Belalia, A. Zehhaf, A. Benyoucef. Preparation of Hybrid Material Based of PANI with SiO_2 and Its Adsorption of Phenol from Aqueous Solution. Polymer Science, Series B. 60 (2018) 816-824.

[32] M. Zenasni, A.Q. Jaime, A. Benyoucef, A. Benghalem. Synthesis and characterization of polymer/V_2O_5 composites based on poly(2-aminodiphenylamine). Polymer Composites. 42 (2021) 1064-1074.

[33] M.H. Sadeghi, M.A. Tofighy, T. Mohammadi. One-dimensional graphene for efficient aqueous heavy metal adsorption: Rapid removal of arsenic and mercury ions by graphene oxide nanoribbons (GONRs). Chemosphere. 253 (2020) 126647.

400 [34] A.B. Wozniak, R. Pietrzak. Adsorption of organic and inorganic pollutants on activated
401 bio-carbons prepared by chemical activation of residues of supercritical extraction of raw
402 plants. Chemical Engineering Journal. 393 (2020) 124785.

403 [35] R.R. Amador, J. Alvarado, G.F. Carrasco, L.M. de la Garza, S.A. Iniesta, A.L. Flores, Y.P.
404 Bernal, M.A.M. Rojas, J.J.G. Arciniega, H.P.M. Hernández, J.F.C. Vega, J.B. Camacho.
405 The Influence of Deposition Time on the Structural, Morphological, Optical and
406 Electrical Properties of ZnO-rGO Nanocomposite Thin Films Grown in a Single Step by
407 USP. Crystals. 10 (2020) 1-21.

408 [36] M. Javed, S.M. Abbas, M. Siddiq, D. Han, L. Niu, Mesoporous silica wrapped with
409 graphene oxide-conducting PANI nanowires as a novel hybrid electrode for
410 supercapacitor. Journal of Physics and Chemistry of Solids. 113 (2018) 220-228.

411 [37] L. Wu, Y. Wu, X. Pan, F. Kong. Synthesis of ZnO nanorod and the annealing effect on its
412 photoluminescence property. Optical Materials. 28 (2006) 418-422.

413 [38] Z. Yang, Q. H. Liu. The structural and optical properties of ZnO nanorods via citric acid-
414 assisted annealing route. Journal of Materials Science. 43 (2008) 6527-6530.

415 [39] W. Bai, Z. Zhang, W. Tian, X. He, Y. Ma, Y. Zhao, Z. Chai. Toxicity of zinc oxide
416 nanoparticles to zebrafish embryo: a physicochemical study of toxicity mechanism.
417 Journal of Nanoparticle Research. 12 (2010) 1645-1654.

418 [40] S. Matindoust, A. Farzi, M.B. Nejad, M.H.S. Abadi, Z. Zou, L.R. Zheng. Ammonia gas
419 sensor based on flexible polyaniline films for rapid detection of spoilage in protein-rich
420 foods. Journal of Materials Science: Materials in Electronics. 28 (2017) 7760-7768.

421 [41] V. Gilja, I. Vrban, V. Mandić, M. Žic, Z.H. Murgić. Preparation of a PANI/ZnO
422 Composite for Efficient Photocatalytic Degradation of Acid Blue. Polymers. 10 (2018) 1-
423 17.

424 [42] C. Bao, M. Chen, X. Jin, D. Hu, Q. Huang. Efficient and stable photocatalytic reduction of
425 aqueous hexavalent chromium ions by polyaniline surface-hybridized ZnO nanosheets.
426 Journal of Molecular Liquids. 279 (2019) 133-145.

427 [43] G. Sriram, U. Uthappa, D. Losic, M. Kigga, H.Y. Jung, M.D. Kurkuri. Mg–Al-Layered
428 Double Hydroxide (LDH) Modified Diatoms for Highly Efficient Removal of Congo Red
429 from Aqueous Solution. Applied Sciences. 10 (2020) 2285.

430 [44] T. Lindfors, A. Ivaska. pH sensitivity of polyaniline and its substituted derivatives. Journal
431 of Electroanalytical Chemistry. 531 (2002) 43-52.

432 [45] H. Zhang, J. Ma, F. Wang, Y. Chu, L. Yang, M. Xia. Mechanism of carboxymethyl
433 chitosan hybrid montmorillonite and adsorption of Pb(II) and Congo red by CMC-MMT
434 organic-inorganic hybrid composite. International Journal of Biological Macromolecules.
435 149 (2020) 1161-1169.

436 [46] A.O. Adesina, O.A. Elvis, N.D.S. Mohallem, S.J. Olusegun. Adsorption of Methylene blue
437 and Congo red from aqueous solution using synthesized alumina–zirconia composite.
438 Environmental Technology . 42 (2021) 1061-1070.

439 [47] C.M. Simonescu, A. Tătăruş, D.C. Culiţă, N. Stănică, I.A. Ionescu, B. Butoi, A.M. Banici.
440 Comparative Study of CoFe2O4 Nanoparticles and CoFe2O4-Chitosan Composite for
441 Congo Red and Methyl Orange Removal by Adsorption. Nanomaterials. 11 (2021) 1-24.

442 [48] R. Wo, Q.L. Li, C. Zhu, Y. Zhang, G.F. Qiao, K.Y. Lei, P. Du, W. Jiang. Preparation and
443 Characterization of Functionalized Metal–Organic Frameworks with Core/Shell Magnetic
444 Particles (Fe3O4@SiO2@MOFs) for Removal of Congo Red and Methylene Blue from
445 Water Solution. Journal of Chemical & Engineering Data. 64 (2019) 2455-2463.

446 [49] C. Aoopngan, J. Nonkumwong, S. Phumying, W. Promjantuek, S. Maensiri, P. Noisa, S.
447 Pinitsoontorn, S. Ananta, L. Srisombat. Amine-Functionalized and Hydroxyl-
448 Functionalized Magnesium Ferrite Nanoparticles for Congo Red Adsorption. ACS
449 Applied Nano Materials. 2 (2019) 5329-5341.

450 [50] H. Chafai, M. Laabd, S. Elbariji, M. Bazzaoui, A. Albourine. Study of congo red
451 adsorption on the polyaniline and polypyrrole. Journal of Dispersion Science and
452 Technology. 38 (2017) 832-836.

453 [51] M.O. Ansari, R. Kumar, S.A. Ansari, S.P. Ansari, M.A. Barakat, A. Alshahrie, M.H. Cho.
454 Anion selective pTSA doped polyaniline@graphene oxide-multiwalled carbon nanotube
455 composite for Cr(VI) and Congo red adsorption. Journal of Colloid and Interface Science.
456 496 (2017) 407-415.

457 [52] R. Kumar, M.O. Ansari, N. Parveen, M.A. Barakat, M.H. Cho. Simple route for the
458 generation of differently functionalized PVC@graphene-polyaniline fiber bundles for the
459 removal of Congo red from wastewater. RSC Adv., 5 (2015) 61486-61494.

460 [53] S. Singh, S. Perween, A. Ranjan. Dramatic enhancement in adsorption of congo red dye in
461 polymer-nanoparticle composite of polyaniline-zinc titanate. Journal of Environmental
462 Chemical Engineering. 9 (2021) 105149

[54] S. Dhananasekaran, R. Palanivel, S. Pappu. Adsorption of Methylene blue, bromophenol blue, and coomassie brilliant blue by α-chitin nanoparticles. Journal of Advanced Research. 7 (2016) 113-124.

[55] D.S. Franco, E.H. Tanabe, D.A. Bertuol, G.S. Dos Reis, E.C. Lima, G.L. Dotto. Alternative treatments to improve the potential of rice husk as adsorbent for methylene blue. Water Sci Technol, 75 (2017) 296-305.

[56] M.O. Bello, N. Abdus-Salam, F.A. Adekola, U. Pal. Isotherm and kinetic studies of adsorption of methylene blue using activated carbon from ackee apple pods. Chemical Data Collections. 31 (2021) 100607

[57] R. Jamal, L. Zhang, M. Wang, Q. Zhao, T. Abdiryim. Synthesis of poly(3,4-propylenedioxythiophene)/MnO2 composites and their applications in the adsorptive removal of methylene blue. Progress in Natural Science: Materials International. 26 (2016) 32-40.

[58] M.M. Ayad, A.A. EI-Nasr. Adsorption of cationic dye (Methylene Blue) from water using polyaniline nanotubes base. Journal of Physical Chemistry C.114 (2010) 14377-14383.

[59] M. Ayad, S. Zaghlol. Nanostructured crosslinked polyaniline with high surface area: synthesis characterization and adsorption for organic dye. Chemical Engineering Journal. 204-206 (2012) 79-86.

Captions

Fig. 1. (a) : Survey XPS spectra ; (b) : FTIR adsorption spectra ; (c) : XRD patterns and (d) : Thermogravimetric analysis obtained in N_2 atmosphere at $10°C.min^{-1}$ of ZnO, PANI and PANI@ZnO.

Fig. 2. SEM images of materials synthetized: (a) ZnO ; (b) PANI and (c) PANI@ZnO.

Fig. 3. (a) : N_2 adsorption & desorption isotherm of adsorbents materials fabricated ; (b) : Effect of pHs on the adsorption capacity of dyes by PANI@ZnO materials (adsorbent dose: 10 mg; dye (CR or MB): 25 mL; T: 298 K) ; (c): Contact Time (C_0: 150 $mg.L^{-1}$; pH: 5.0; T: 298K; adsorbents dose: 10 mg) ; (d): Adsorption isotherms of dyes by nanomaterial (adsorbent dose: 10 mg; dye (CR or MB): 25 mL; T: 298 K; pH: 5.0).

Fig. 4. Adsorbent capacity changes and initial dyes (CR and MB) in consecutive cycles (adsorbent dose: 10 mg; dye (CR or MB): 25 mL; T: 298 K; pH: 5.0).

Figures

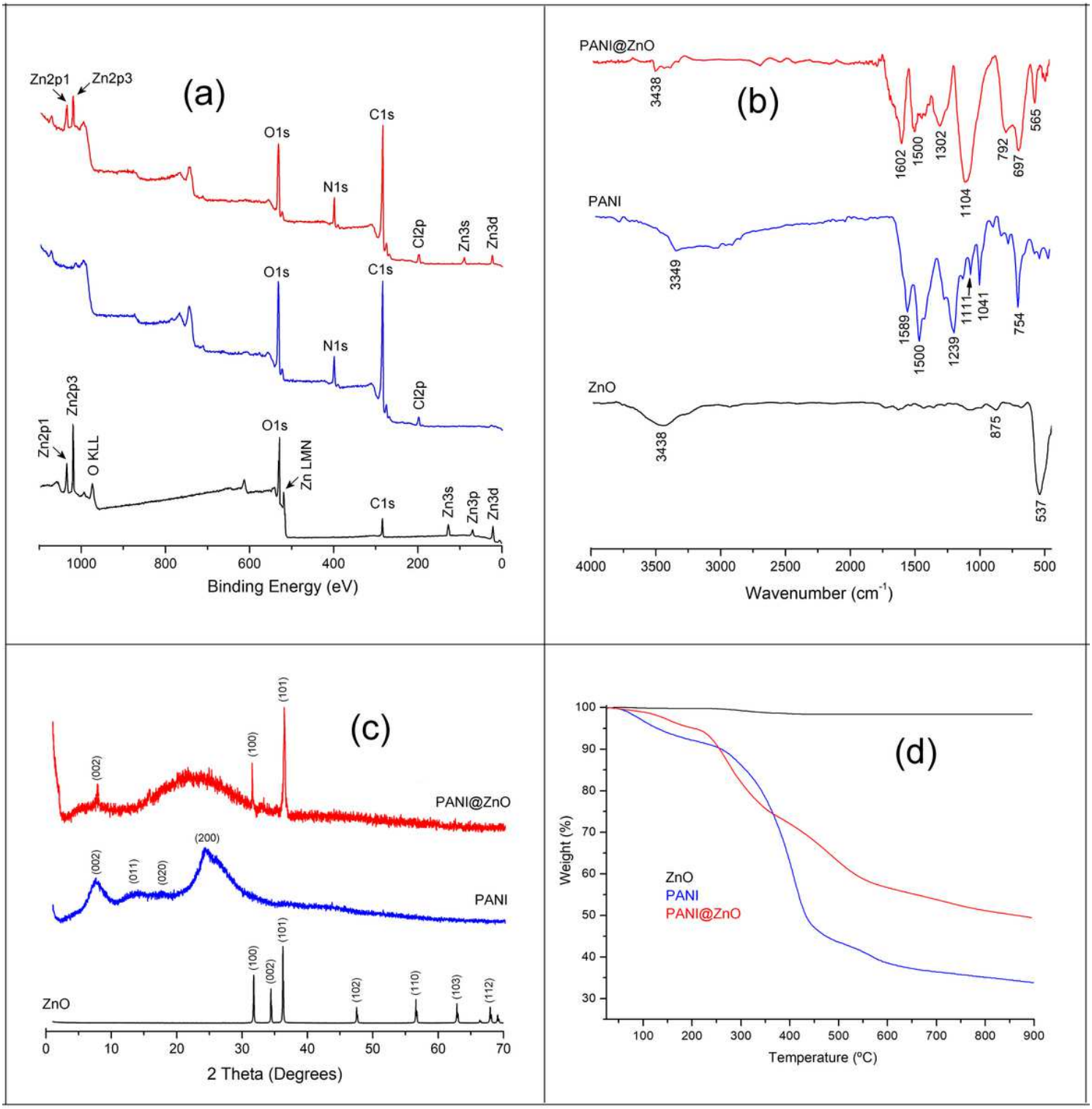

Figure 1

(a) : Survey XPS spectra ; (b) : FTIR adsorption spectra ; (c) : XRD patterns and (d) : Thermogravimetric analysis obtained in N2 atmosphere at 10°C.min-1 of ZnO, PANI and PANI@ZnO.

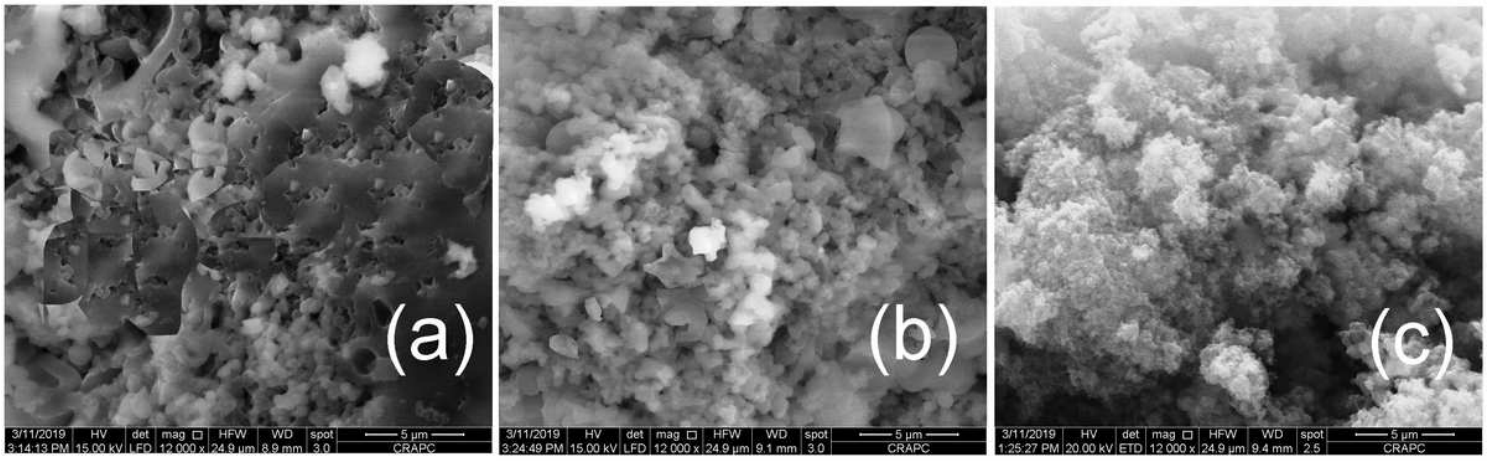

Figure 2

SEM images of materials synthetized: (a) ZnO ; (b) PANI and (c) PANI@ZnO.

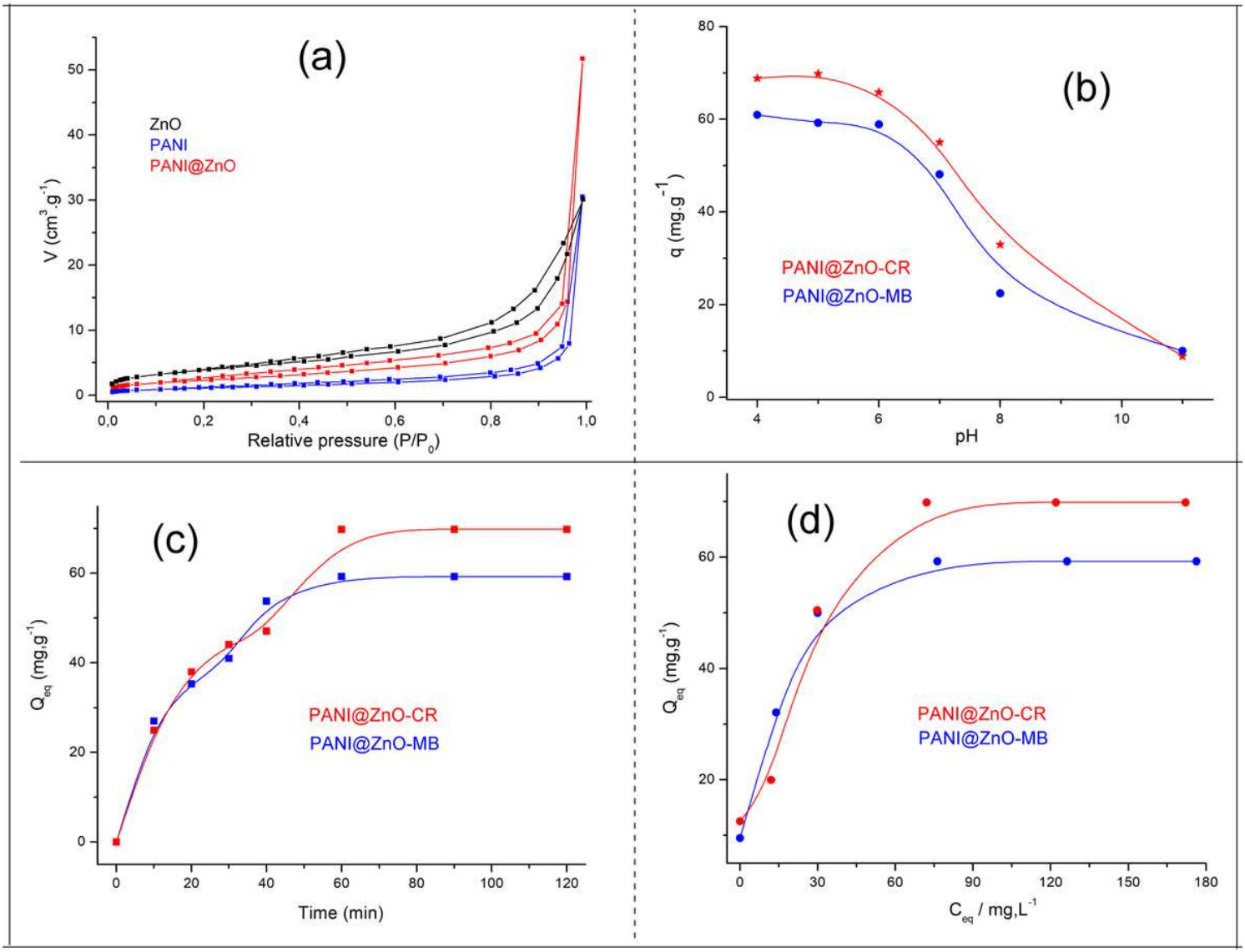

Figure 3

(a) : N2 adsorption & desorption isotherm of adsorbents materials fabricated ; (b) : Effect of pHs on the adsorption capacity of dyes by PANI@ZnO materials (adsorbent dose: 10 mg; dye (CR or MB): 25 mL; T: 298 K) ; (c): Contact Time (C0: 150 mg.L-1; pH: 5.0; T: 298K; adsorbents dose: 10 mg) ; (d): Adsorption isotherms of dyes by nanomaterial (adsorbent dose: 10 mg; dye (CR or MB): 25 mL; T: 298 K; pH: 5.0).

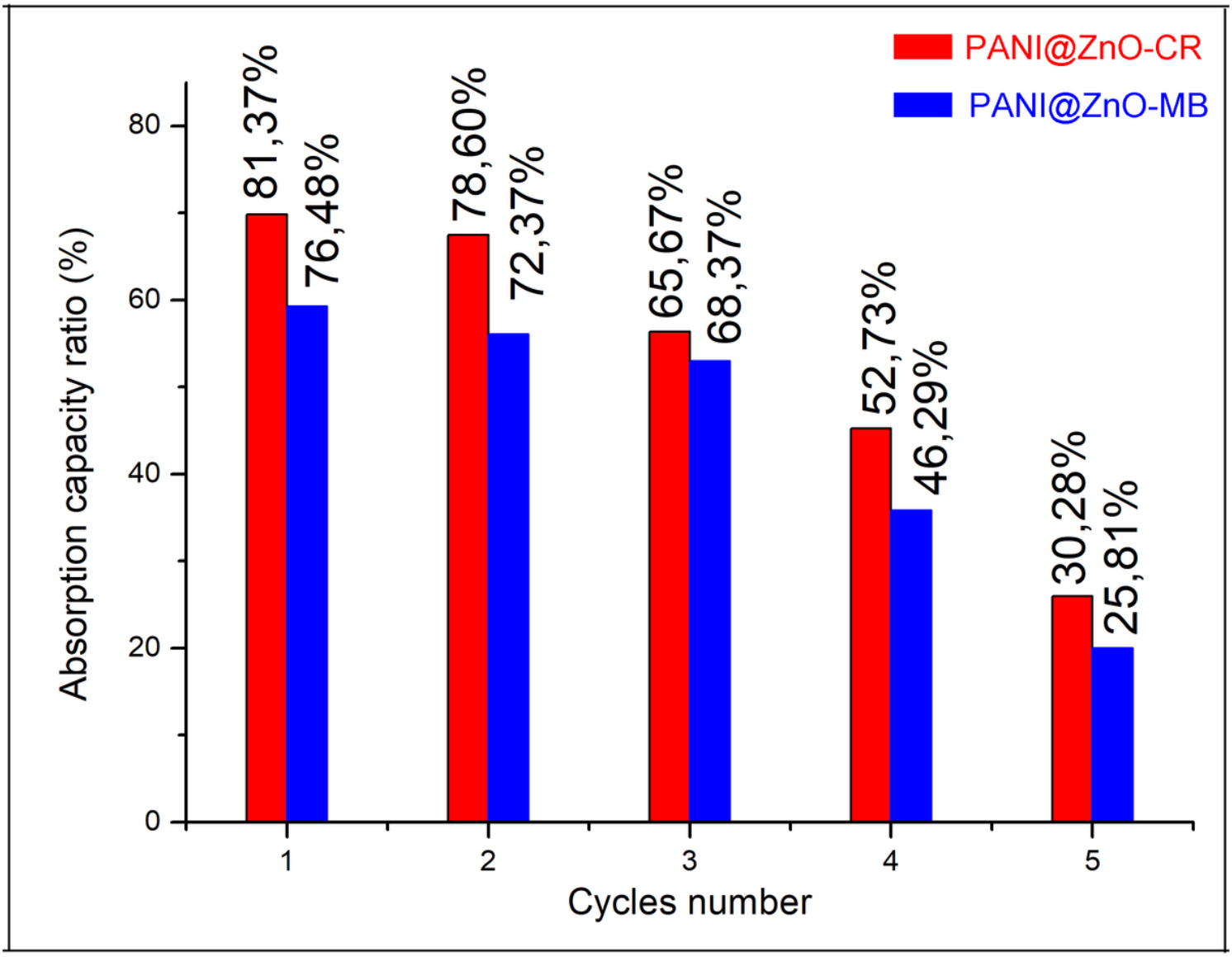

Figure 4

Adsorbent capacity changes and initial dyes (CR and MB) in consecutive cycles (adsorbent dose: 10 mg; dye (CR or MB): 25 mL; T: 298 K; pH: 5.0).